Wireless Solar Water Splitting Using Silicon-Based Semiconductors and Earth-Abundant Catalysts

Steven Y. Reece *et al.*

Science **334**, 645 (2011);
DOI: 10.1126/science.1209816

Science (print ISSN 0036-8075; online ISSN 1095-9203) is published weekly, except the last week in December, by the American Association for the Advancement of Science, 1200 New York Avenue NW, Washington, DC 20005.

Wireless Solar Water Splitting Using Silicon-Based Semiconductors and Earth-Abundant Catalysts

Steven Y. Reece,[1]* Jonathan A. Hamel,[1] Kimberly Sung,[1] Thomas D. Jarvi,[1]* Arthur J. Esswein,[1] Joep J. H. Pijpers,[2,3] Daniel G. Nocera[2]*

We describe the development of solar water-splitting cells comprising earth-abundant elements that operate in near-neutral pH conditions, both with and without connecting wires. The cells consist of a triple junction, amorphous silicon photovoltaic interfaced to hydrogen- and oxygen-evolving catalysts made from an alloy of earth-abundant metals and a cobalt|borate catalyst, respectively. The devices described here carry out the solar-driven water-splitting reaction at efficiencies of 4.7% for a wired configuration and 2.5% for a wireless configuration when illuminated with 1 sun (100 milliwatts per square centimeter) of air mass 1.5 simulated sunlight. Fuel-forming catalysts interfaced with light-harvesting semiconductors afford a pathway to direct solar-to-fuels conversion that captures many of the basic functional elements of a leaf.

Although solar photovoltaic (PV) cells normally generate electricity, they can be used to generate fuels such as hydrogen from water, thus providing a storage mechanism for sunlight (*1*). Such schemes mimic the photosynthetic process within a leaf that converts the energy of sunlight into chemical energy by splitting water to produce O_2 and hydrogen equivalents (*2*). The primary steps of natural photosynthesis involve the absorption of sunlight and its conversion into spatially separated electron-hole pairs. The holes of this wireless current are captured by the oxygen-evolving complex (OEC) of Photosystem II (PSII) to split H_2O to O_2. The electrons and protons produced as the by-products of the OEC reaction are transferred to Photosystem I (PSI) to produce a reduced form of hydrogen in the form of NADPH (the reduced form of nicotinamide adenine dinucleotide phosphate) (*2*). The separation of light collection/conversion from catalysis is compulsory to the photosynthetic function because electron/hole pairs are generated one at a time and the water splitting reaction is a four electron-hole process (*3*). The multielectron catalysts of PSII and PSI are therefore needed to bridge the light-driven one electron-hole "wireless current" of the light collection and conversion apparatus of the leaf to the four electron-hole chemistry of water splitting.

A general approach for mimicking photosynthesis is to generate O_2 and H_2 with inorganic materials using fuel-forming catalysts interfaced with light-harvesting semiconductors (*4*–*6*). Sunlight is absorbed by the semiconductor and generates spatially separated electron-hole pairs. The electron-hole pairs of this wireless current are captured with two catalysts that drive the water-splitting reaction under near-neutral pH conditions. A system of this type must generate electrons and holes with enough energy to overcome both the energetic barrier of water oxidation (1.23 V at standard conditions) and any overpotentials needed to drive catalysis. Wireless photochemical cells (*7*, *8*) and wired photoelectrochemical cells (PECs) (*9*–*14*) for solar-powered water splitting have been realized, but practical problems remain. Schemes for solar photochemical production of H_2 and O_2 from water at reasonable efficiency have relied on the use of prohibitively expensive light-absorbing materials [e.g., (Al)GaAs and GaInP], and/or fuel-forming catalysts (e.g., Pt, RuO_2, IrO_2), and strongly acidic or basic reaction media, which are corrosive and expensive to manage over the large areas required for light harvesting. A focus of current research has been to mimic photosynthesis with materials composed of earth-abundant elements in electrolytes near neutral pH conditions (*15*). The success of this approach will enable novel PEC and other light-harvesting (e.g., wireless) architectures to be engineered to produce solar fuel at more practical cost targets.

Silicon is an attractive materials choice for constructing an artificial leaf because of its earth-abundance and prevalence in the electronics and PV industries. The realization of a direct solar-to-fuel device based on silicon, however, must overcome the inherent corrosion of this semiconductor in nonacid electrolytes (*16*). Previous stand-alone, water-splitting PEC configurations have physically shielded the silicon from the electrolyte and used wires (*7*, *11*) or a conductive oxide (*12*, *13*) to connect the semiconductor to the hydrogen- and/or oxygen-generating electrodes. Tunneling oxide layers have also been explored recently to stabilize wired silicon photoanodes (*17*). These approaches limit the application of Si in photochemical water splitting to a traditional, wired PEC panel geometry, which has traditionally proved too costly for commercialization.

We show that water-splitting catalysts comprising earth-abundant materials can be integrated with amorphous silicon with minimal engineering to enable direct solar-to-fuels conversion based on water splitting. For the O_2-evolving catalyst, we use a cobalt catalyst (*18*), Co-OEC, that self-assembles upon oxidation of Co^{2+} (*19*), self-heals (*20*), and can operate in buffered electrolyte with pure or natural water at room temperature (*21*, *22*). These attributes are similar to those of the OEC found in photosynthetic organisms. Moreover, x-ray absorption spectroscopy (*23*, *24*) has established that the Co-OEC is a structural relative of Mn_3CaO_4–Mn cubane (*25*–*27*) of the OEC of PSII, where Co replaces Mn and the cubane is extended in a corner-sharing head-to-tail dimer (*28*). It has been established that the Co-OEC, when interfaced to semiconductors, enhances the efficiency of solar-assisted water splitting (*29*–*33*). The H_2-evolving catalyst is a ternary alloy, NiMoZn. These catalysts have been interfaced directly with a commercial triple-junction amorphous silicon (3jn-a-Si) solar cell (Xunlight Corp.) in wired and wireless configurations. For either, the cell uses stacked amorphous silicon and amorphous silicon-germanium alloy junctions deposited on a stainless steel substrate and coated with a 70-nm layer of indium tin oxide (ITO) (*34*). Although the abundance of Ge may be a source of debate (*35*), the use of a silicon-based light absorber represents a major step toward a device composed of all earth-abundant materials for solar water splitting. Co-OEC is deposited directly onto the ITO layer (the illuminated side of the cell). The NiMoZn alloy H_2 catalyst was used in two configurations: (i) deposited on a Ni mesh substrate that is wired to the 3jn-a-Si solar cell and (ii) deposited directly on the opposing stainless steel surface of the 3jn-a-Si solar cell as a wireless device. The devices, which have not been optimized for performance, may operate out of an open container of water containing borate electrolyte and with overall direct solar-to-fuels efficiencies of 2.5% (wireless) and 4.7% (wired) when driven by a solar cell of 6.2% and 7.7% light-to-electricity efficiency, respectively. The overall conversion efficiency of the wired cell indicates that a majority of the power from the solar cell can be converted directly to solar fuels and that a simply engineered, functional artificial leaf comprising earth-abundant materials may be realized.

The PEC properties of the unmodified solar cell were characterized by operation of the cell as a photoanode in a three-electrode voltammetry configuration (3jn-a-Si working electrode, Pt counter electrode, and Ag/AgCl reference electrode). Figure 1A plots the current densities obtained from the photoanode as a function of the applied potential, illumination, and electrolyte conditions. In the absence of light (Fig. 1A, gray trace), a low anodic current density ($j < 0.05$ mA/cm^2) was observed upon sweeping the 3jn-

[1]Sun Catalytix, Cambridge, MA 02139, USA. [2]Department of Chemistry, Massachusetts Institute of Technology, Cambridge, MA 02139–4307, USA. [3]Foundation for Fundamental Research on Matter, Institute for Atomic and Molecular Physics, Science Park 104, 1098 XG, Amsterdam, Netherlands.

*To whom correspondence should be addressed. E-mail: nocera@mit.edu (D.G.N.); streece@suncatalytix.com (S.Y.R.); tjarvi@suncatalytix.com (T.D.J.)

a-Si anode from negative to positive potentials for $E > 0.02$ V versus the reversible hydrogen electrode (RHE) (*36*). The onset potential (E_{on}) of this sweep may be defined as the potential at which the current changes from positive (cathodic) to negative (anodic) values. Upon illumination of the cell with 1 sun (100 mW/cm^2) of air mass (AM) 1.5 simulated sunlight (Fig. 1A, black trace) in 1 M potassium borate electrolyte (pH 9.2), E_{on} shifted to more negative values and the magnitude of the anodic current (j_{an}) increased slightly ($E_{on} = -0.14$ V versus RHE, and $j_{max,an} = 0.39$ mA/cm^2 at 0.55 V versus RHE, the most positive potential of the sweep). The photoanode current of the ITO-coated solar cell was limited under illumination in this configuration because water splitting does not occur appreciably in the absence of catalysts.

Upon addition of 0.25 mM Co^{2+}(aq) to the borate electrolyte, E_{on} shifted to a more negative value (−0.37 V versus RHE) and the anodic current density increased dramatically (j_{an} = 4.17 mA/cm^2 at 0.55 V versus RHE) (Fig. 1A, red trace). Illumination (AM 1.5) of the cell under these conditions at fixed potential ($E = -0.26$ V versus RHE) caused a thin film to form on the electrode, and the current-time trace observed in Fig. 1B was obtained. The photocurrent rose and reached a plateau at a value of 1.5 mA/cm^2 during the 12-min course of the experiment, concomitant with the evolution of bubbles at both the photoanode surface and the Pt wire counter electrode. Gas chromatography experiments identified the evolved gases to be H_2 and O_2. Upon completion of the photoelectrolysis experiment, the surface coloration of the cell changed from purple to light blue, which we ascribed to the formation of a thin film of the Co-OEC on the surface of the cell (see below). We attribute the rise in current in Fig. 1B to the deposition of the Co-OEC catalyst and to water splitting. The activity of the photoanode increased with Co-OEC loading, but a tradeoff existed as the catalyst layer grew thicker and blocked more of the incident radiation. Thus, short deposition times (~5 min) yielded photoanodes with optimum performance; the presence of borate maintains the optimal film thickness and preserves the self-healing properties of the catalyst.

The Co-OEC | 3jn-a-Si photoelectrodes were characterized by scanning electron microscopy (SEM) and energy-dispersive x-ray (EDX) analysis. We coated solar cells with both thin (5-min deposition time) and thick (1-hour deposition time) Co-OEC film layers. SEM analysis of cross sections (Fig. 2) allowed for determination of the thickness of the dried catalyst layer (thin film average, 85 nm; thick film average, 200 nm) and the thickness of the 3jn-a-Si layer (~1 μm); the average film thicknesses were provided from several measurements. Low-energy EDX analysis was performed to estimate the elemental composition of the substrate surface, as compared to the pristine 3jn-a-Si cell (fig. S1). Cobalt was observed only for solar cells coated with Co-OEC films, and the signal for Co was more intense for the sample with thicker Co-OEC films.

We characterized the performance of the photoanode with a Co-OEC film in the absence of Co^{2+} in the electrolyte. The performance of the 3jn-a-Si coated with the 85-nm-thick films of Co-OEC was assessed in solutions containing 1 M potassium borate electrolyte. The Co-OEC | 3jn-a-Si cell exhibits a negative shift in the onset potential ($E_{on} = -0.40$ V versus RHE) and enhanced anodic photocurrents ($j_{an} = 4.4$ mA/cm^2), relative to an uncatalyzed 3jn-a-Si cell ($E_{on} = -0.14$ V versus RHE; $j_{an} = 0.4$ mA/cm^2). The degree to which the Co-OEC film blocked incoming light and inhibited the PV performance of the cell was assessed by measuring the current-voltage curve in air under AM 1.5 illumination (fig. S2). Under these conditions, the 3jn-a-Si cell functioned as a pure PV cell and not a PEC. Due to deposition of the Co-OEC film, the short-circuit current (j_{SC} = current at zero applied bias) decreased from 6.5 to 5.9 mA/cm^2, and the fill factor decreased from 0.57 to 0.50. Thus, the catalyst film of 85 nm decreased the PV performance by ~9% (8.0% to 7.3% for light-to-electricity conversion efficiency). The precision of our measurements for a given experiment is high (<1% error); the data presented are for the highest performing cells.

Stand-alone operation of the cell with no external applied potential from an electrical power source (i.e., unassisted) was performed by using the Co-OEC | 3jn-a-Si photoanode in conjunction with the NiMoZn cathode for H_2 production. This earth-abundant H_2 evolution catalyst was electrodeposited as described in the supporting online material (SOM). Figure S3 compares the activity of the ternary alloy, as deposited (*37*), and bare Ni metal in 1 M potassium borate (pH 9.2). Over the potential range of the experiment, the alloy generated 50 times as much current as smooth Ni metal for the same geometric surface area. When used in conjunction with the Co-OEC | 3jn-a-Si photoanode, the NiMoZn was deposited on a Ni wire mesh substrate that was wired to the steel substrate of the 3jn-a-Si cell and placed between the light source and the photoanode. The cell, which is schematically depicted in Fig. 3A, was illuminated with AM 1.5 solar-simulated light, and the solar-to-fuels efficiency

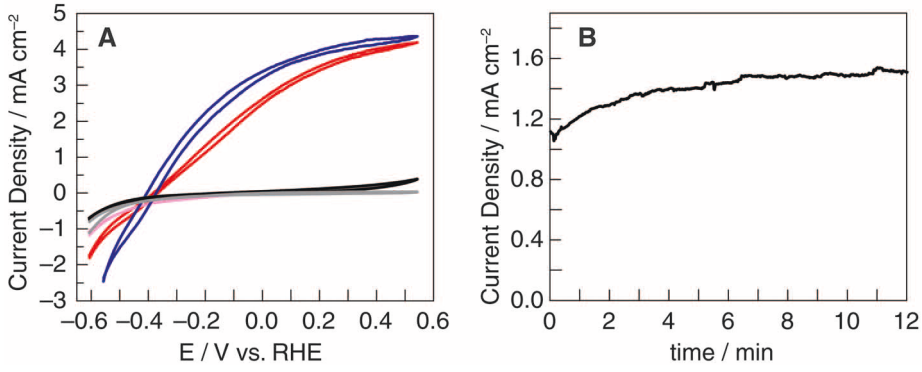

Fig. 1. (**A**) Current-voltage plot of the 3jn-a-Si photoanode: in the dark (gray trace); under AM 1.5 illumination (1 sun) (black trace); in the presence of 0.25 mM Co^{2+} in the dark (pink trace) and (red trace) under 1 sun; and coated with a Co-OEC film under 1 sun (blue trace). The 3jn-a-Si cell was the working electrode of a three-electrode configuration (Pt counter electrode, Ag/AgCl reference electrode, 1 M potassium borate electrolyte, pH 9.2). Potentials were scanned from negative to positive to negative values. (**B**) Bulk photoelectrolysis plot (current density versus time) during photodeposition of the Co-OEC film from 0.25 mM Co^{2+} and 1 M potassium borate (pH 9.2) under 1 sun illumination. The 3jn-a-Si photoanode was held at −0.26 V versus RHE.

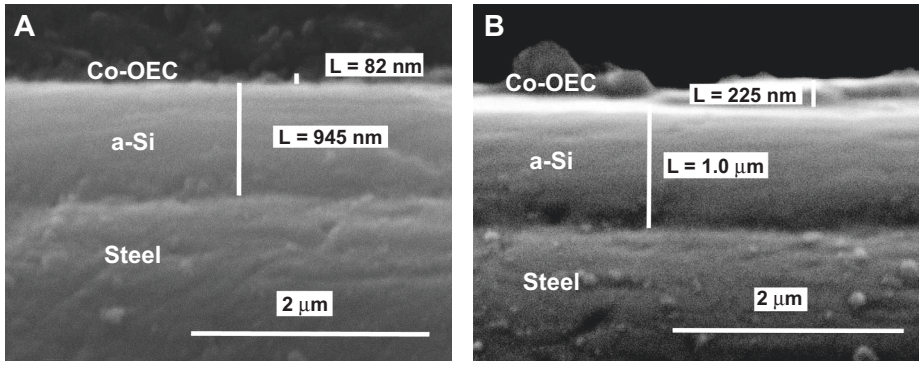

Fig. 2. SEM of cross sections of the Co-OEC | 3jn-a-Si cell after (**A**) 5 min and (**B**) 1 hour deposition of the Co-OEC film.

(SFE) for conversion of light and water into H_2 and O_2 was calculated using Eq. 1 (*15*),

$$\mathrm{SFE}(\%) = j \bullet \Delta E / S \bullet 100\% = J\,(\mathrm{mA/cm^2}) \bullet 1.23\ \mathrm{V} / 100\ (\mathrm{mW/cm^2}) \bullet 100\% \quad (1)$$

where j is the current density at the photoelectrode, ΔE is the stored energy of the water-splitting reaction, and S is the total incident solar irradiance, which is provided by the AM 1.5 light source at 100 mW/cm^2. Figure 3A plots the efficiency and stability of Co-OEC | 3jn-a-Si | NiMoZn PEC cells operated in 1 M KBi (black trace) and 0.1 M KOH (red trace) electrolyte. The overall performance of the water-splitting cells was directly correlated to their intrinsic performance of the specific underlying PV sample. In Fig. 3A, the 3jn-a-Si PV solar cell was 7.7% efficient and yielded an overall PEC cell efficiency of 4.7% (Fig. 3A, black trace). We note that light passed through the mesh, which has a transmittance of ~85% (the efficiency reported here has not been corrected for light blocking by the mesh). Electrolysis efficiencies improved slightly upon operation of the cell in 0.1 M KOH electrolyte because of an increase in catalyst activity (Fig. 3A); however, the use of this electrolyte resulted in a rapid and catastrophic decline in activity after 1 hour of photolysis (Fig. 3A, red trace), concomitant with visible dissolution of the 3jn-a-Si layer. This phenomenon had been previously observed and attributed to pitting corrosion of the ITO coating by the KOH electrolyte (*12*). Conversely, the Co-OEC | 3jn-a-Si | NiMoZn cell exhibited significantly enhanced stability in borate electrolyte (Figure 3A, black trace). O_2 yields were measured with a phosphorescence-based O_2 sensor (fig. S4) and showed that virtually all of the electron-holes created during photoelectrolysis were used to convert water into O_2 at the anode (within the 5% error of the measurement).

The SFE may also be expressed as a direct product of the efficiency of the solar conversion of the PV cell, φ(PV), and fuel generation efficiency of water-splitting electrolysis, φ(WS), which includes losses that arise from catalyst overpotentials and Ohmic resistances,

$$\mathrm{SFE}\ (\%) = \varphi(\mathrm{PV}) \bullet \varphi(\mathrm{WS}) \quad (2)$$

Thus, φ(WS) is calculated to be ~60%. This value compares well with cell efficiencies based on 3jn-a-Si PVs in which the a-Si is isolated from the electrolyte [SFE = 6% for φ(PV) = 10%] (*7*, *11*, *12*) and for higher-efficiency systems using expensive PV materials [SFE = 18% for φ(PV) = 28%] (*7*–*9*). We note that, based on φ(WS), higher overall cell efficiencies (>10%) may be readily achieved through the use of more efficient PVs (*38*).

A wireless cell was constructed by deposition of the H_2-evolving catalyst, NiMoZn, onto the steel-backing substrate of the 3jn-a-Si cell. The overall device architecture is illustrated in Fig. 3B. Movie S1 shows the operation of a 1 × 2 cm^2 wireless Co-OEC | 3jn-a-Si | NiMoZn wafer that was immersed in an open container of electrolyte (1 M potassium borate, pH 9.2) and illuminated with 1 sun, AM 1.5 simulated sunlight. The cell architecture dictated that O_2 bubbles evolved from the illuminated anode at the front face (5 to 47 s of movie S1) and bubbles of H_2 evolved from the cathode at the back of the wireless cell (47 to 102 s of movie S1).

Oxygen yields (Fig. 3B) were determined through operation in an electrochemical cell in a closed configuration, in which the produced gases were analyzed using a mass spectrometer (MS). For this experiment, an Ar carrier gas was flowed over the headspace of the cell at a constant flow rate. The MS signal corresponds to the concentration of O_2 in the carrier gas, which was used to determine the SFE for the wireless cell (see SOM for experimental details); a SFE = 1.75% was measured for a 3jn-a-Si solar cell with φ(PV) = 6.2%. Based on the PEC cell of φ(PV) = 7.7%, we expect that minimal efficiencies of 4.7% may be obtained from a properly engineered wireless cell. For instance, in the present wireless cell configuration, protons generated at the front face of the anode must move around to the back side of the cell, where they are reduced at the cathode to H_2. These relatively long distances for ion transport impose substantial Ohmic losses in the cell, resulting in lower φ(WS). These losses may be mitigated by increasing the conductance of the solution. For instance, substituting the 1 M KBi electrolyte (specific conductivity = 26 mS/cm) with a mixture of 0.5 M KBi and 1.5 M KNO_3 (specific conductivity = 126 mS/cm) resulted in an increase in the SFE from 1.75 to 2.5% (Fig. 3B). In addition, future designs (e.g., flow cell or perforated Si cell) could increase the SFE further by decreasing the anode-cathode ion transport distance and bring the wireless cell performance closer to that of the wired PEC cell, which has a 1-mm gap between cathode and anode (Fig. 3A).

The stability of the wireless cells was assessed by monitoring the O_2 MS signal of a wireless

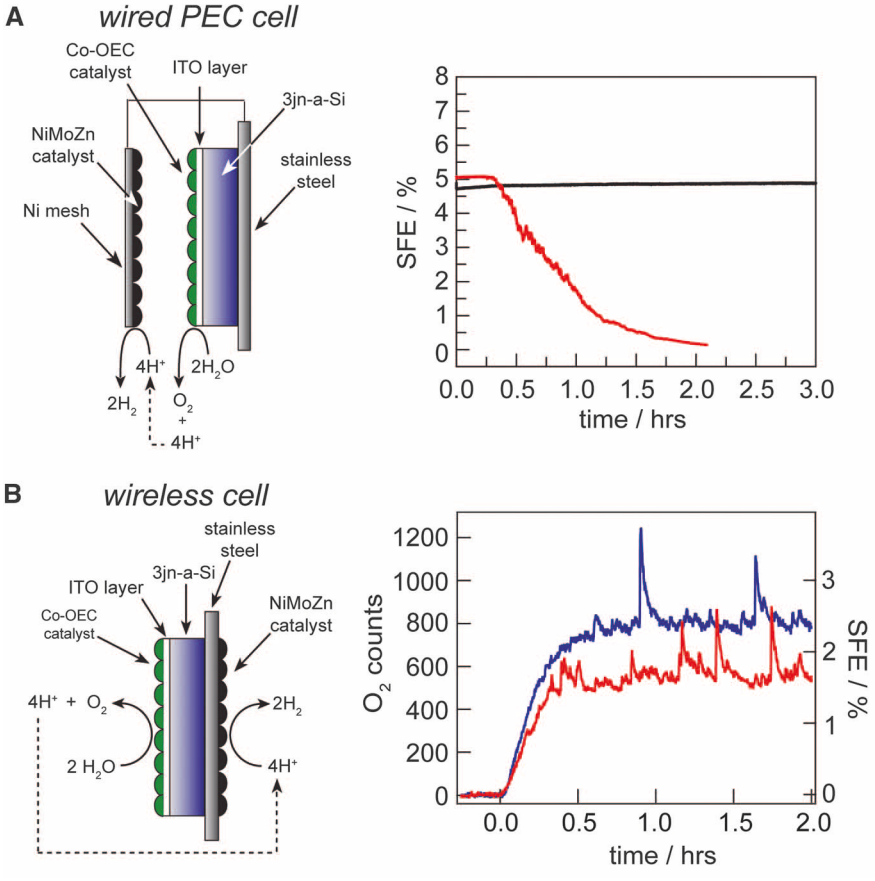

Fig. 3. (**A**) Plot of the efficiency versus time for Co-OEC | 3jn-a-Si | NiMoZn PEC cell (left) in 1 M potassium borate (pH 9.2, black trace) and in 0.1 M KOH (pH 13, red trace) under AM 1.5 illumination. The traces are for solar cells of 7.7% PV efficiency. The cells were operated in a two-electrode cell configuration. (**B**) MS signal and SFE values for a wireless Co-OEC | 3jn-a-Si | NiMoZn cell under AM 1.5 illumination in 1 M KBi (red trace) and in 0.5 M KBi and 1.5 M KNO_3 (blue trace). The cell was illuminated over the 2 hours of the experiment; MS signal corresponds to the concentration of O_2 in the carrier gas of the cell. The spikes in the data originate from sudden release of gas bubbles that were adhered to the cells, resulting in a temporary increase of the O_2 concentration in the headspace. SFE values were calculated as described in the SOM.

cell operating in 1 M KBi (fig. S5A). The cell was stable for 10 hours, after which its performance gradually declined to ~80% of its initial value over 24 hours. We have found that the stability of the cell is directly related to the nature of and preparative method for the transparent conductive oxide barrier layer. For example, fluorine-doped tin oxide (FTO), when prepared and annealed on crystalline Si at high temperatures (see SOM for experimental details), results in a PEC cell with stable performance over 30 hours of testing (fig. S5B), suggesting that cells using crystalline Si with the catalysts described here have great practical value. Similar strategies may be applied for protection of the 3jn-a-Si cell; however, we note that they must be compatible with the low-temperature manufacturing conditions of 3jn-a-Si.

The integration of earth-abundant water-splitting catalysts with photovoltaic silicon cells captures the functional elements of energy capture and storage by a leaf. The ability to drive water splitting directly without the use of wires under a simply engineered configuration opens new avenues of exploration. For instance, the design described here could be adapted from a panel geometry to one based on freestanding (nano)particles in solution. Moreover, owing to the low solubility of O_2 and H_2 in water, the solar-to-fuels conversion process may be driven in the absence of a membrane. The H_2 produced by photochemical water splitting may be collected directly and used or combined with carbon dioxide in a synthetic liquid fuels process external to the cell. By constructing a simple, stand-alone device composed of silicon-based light absorbers and earth-abundant catalysts, the results described here provide a first step down a path aligned with the low-cost systems engineering and manufacturing (*39*) that is required for inexpensive direct solar-to-fuels systems.

References and Notes

1. T. R. Cook *et al.*, *Chem. Rev.* **110**, 6474 (2010).
2. J. Barber, *Phil. Trans. Roy. Soc. A* **365**, 1007 (2007).
3. T. A. Betley, Q. Wu, T. Van Voorhis, D. G. Nocera, *Inorg. Chem.* **47**, 1849 (2008).
4. N. S. Lewis, D. G. Nocera, *Proc. Natl. Acad. Sci. U.S.A.* **103**, 15729 (2006).
5. D. G. Nocera, *ChemSusChem* **2**, 387 (2009).
6. D. Abbott, *Proc. IEEE* **98**, 42 (2010).
7. O. Khaselev, A. Bansal, J. A. Turner, *Int. J. Hydrogen Energy* **26**, 127 (2001).
8. G. H. Lin, M. Kapur, R. C. Kainthla, J. O. M. Bockris, *Appl. Phys. Lett.* **55**, 386 (1989).
9. O. Khaselev, J. A. Turner, *Science* **280**, 425 (1998).
10. S. Licht *et al.*, *J. Phys. Chem. B* **104**, 8920 (2000).
11. R. E. Rocheleau, E. L. Miller, A. Misra, *Energy Fuels* **12**, 3 (1998).
12. N. A. Kelly, T. L. Gibson, *Int. J. Hydrogen Energy* **31**, 1658 (2006).
13. T. L. Gibson, N. A. Kelly, U.S. Patent 7,052,587 (2003).
14. A. E. Delahoy, S. C. Gau, O. J. Murphy, M. Kapur, J. O. M. Bockris, *Int. J. Hydrogen Energy* **10**, 113 (1985).
15. M. G. Walter *et al.*, *Chem. Rev.* **110**, 6446 (2010).
16. X. G. Zhang, *Silicon and Its Oxide* (Kluwer Academic, New York, 2001).
17. Y. W. Chen *et al.*, *Nat. Mater.* **10**, 539 (2011).
18. M. W. Kanan, D. G. Nocera, *Science* **321**, 1072 (2008).
19. Y. Surendranath, M. W. Kanan, D. G. Nocera, *J. Am. Chem. Soc.* **132**, 16501 (2010).
20. D. A. Lutterman, Y. Surendranath, D. G. Nocera, *J. Am. Chem. Soc.* **131**, 3838 (2009).
21. Y. Surendranath, M. Dincă, D. G. Nocera, *J. Am. Chem. Soc.* **131**, 2615 (2009).
22. A. J. Esswein, Y. Surendranath, S. Y. Reece, D. G. Nocera, *Energy Environ. Sci.* **4**, 499 (2011).
23. M. Risch *et al.*, *J. Am. Chem. Soc.* **131**, 6936 (2009).
24. M. W. Kanan *et al.*, *J. Am. Chem. Soc.* **132**, 13692 (2010).
25. J. Barber, *Inorg. Chem.* **47**, 1700 (2008).
26. E. M. Sproviero, J. A. Gascon, J. P. McEvoy, G. W. Brudvig, V. S. Batista, *J. Am. Chem. Soc.* **130**, 6728 (2008).
27. Y. Umena, K. Kawakami, J.-R. Shen, N. Kamiya, *Nature* **473**, 55 (2011).
28. M. D. Symes, Y. Surendranath, D. A. Lutterman, D. G. Nocera, *J. Am. Chem. Soc.* **133**, 5174 (2011).
29. J. A. Seabold, K. S. Choi, *Chem. Mater.* **23**, 1105 (2011).
30. E. M. P. Steinmiller, K. S. Choi, *Proc. Natl. Acad. Sci. U.S.A.* **106**, 20633 (2009).
31. D. K. Zhong, J. Sun, H. Inumaru, D. R. Gamelin, *J. Am. Chem. Soc.* **131**, 6086 (2009).
32. D. K. Zhong, D. R. Gamelin, *J. Am. Chem. Soc.* **132**, 4202 (2010).
33. D. K. Zhong, M. Cornuz, K. Sivula, M. Grätzel, D. R. Gamelin, *Energy Environ. Sci.* **4**, 1759 (2011).
34. X. Deng, E. A. Schiff, in *Handbook of Photovoltaic Science and Engineering*, A. Luque, S. Hegedus, Eds. (Wiley, Chichester, England, 2003), pp. 505–565.
35. Germanium commodity summary, U.S. Geological Survey; available online at http://minerals.usgs.gov/minerals/pubs/commodity/germanium/mcs-2011-germa.pdf.
36. The RHE potential is that of the standard hydrogen electrode (SHE) adjusted for the pH of the solution. Potentials (versus RHE) were calculated from the measured values (versus Ag/AgCl) according to the equation $E(\mathrm{RHE}) = E(\mathrm{Ag/AgCl}) + 0.197\mathrm{V} + (0.059\mathrm{V} \times \mathrm{pH})$.
37. Mo leaches from alloys to furnish high-surface-area materials; thus, the activity of the alloy increases with leaching time [see (*40*, *41*)]. After 9 days, leaching ceases and a very active, high-surface-area material is obtained.
38. J. J. H. Pijpers, M. T. Winkler, Y. Surendranath, T. Buonassisi, D. G. Nocera, *Proc. Natl. Acad. Sci. U.S.A.* **108**, 10056 (2011).
39. B. D. James, G. N. Baum, J. Perez, K. N. Baum, U.S. Department of Energy, Dec. 2009. Available online at: http://www1.eere.energy.gov/hydrogenandfuelcells/pdfs/pec_technoeconomic_analysis.pdf.
40. B. E. Conway, L. Bai, *Int. J. Hydrogen Energy* **11**, 533 (1986).
41. J. Z. O. Stachurski, D. Pouli, J. A. Ripa, G. F. Pokrzyk, U.S. Patent 4,354,915 (1982).

Acknowledgments: Sun Catalytix acknowledges Xunlight Corporation for providing the 3jn-a-Si cells and ARPA-E (DE-AR0000036) for funding. D.G.N. acknowledges support with grants from the National Science Foundation (CHE-0533150), AFOSR FA9550-09-1-0689, and the Chesonis Family Foundation. J.J.H.P. performed work as part of the Fellowships for Young Energy Scientists program of the Foundation for Fundamental Research on Matter (FOM), which is financially supported by the Netherlands Organization for Scientific Research (NWO). NWO is also gratefully acknowledged for supplying a Rubicon grant to J.J.H.P. J. Turner and E. Miller are acknowledged for helpful discussions.

Supporting Online Material

www.sciencemag.org/cgi/content/full/science.1209816/DC1
Materials and Methods
Figs. S1 to S5
Movie S1

15 June 2011; accepted 15 September 2011
Published online 29 September 2011;
10.1126/science.1209816

Hot Carrier–Assisted Intrinsic Photoresponse in Graphene

Nathaniel M. Gabor,[1] Justin C. W. Song,[1,2] Qiong Ma,[1] Nityan L. Nair,[1] Thiti Taychatanapat,[1,3] Kenji Watanabe,[4] Takashi Taniguchi,[4] Leonid S. Levitov,[1] Pablo Jarillo-Herrero[1]*

We report on the intrinsic optoelectronic response of high-quality dual-gated monolayer and bilayer graphene p-n junction devices. Local laser excitation (of wavelength 850 nanometers) at the p-n interface leads to striking six-fold photovoltage patterns as a function of bottom- and top-gate voltages. These patterns, together with the measured spatial and density dependence of the photoresponse, provide strong evidence that nonlocal hot carrier transport, rather than the photovoltaic effect, dominates the intrinsic photoresponse in graphene. This regime, which features a long-lived and spatially distributed hot carrier population, may offer a path to hot carrier–assisted thermoelectric technologies for efficient solar energy harvesting.

The photoresponse of semiconductors, which determines the performance of optoelectronic devices, is governed by energy relaxation pathways of photoexcited electron-hole pairs: Energy transferred to the lattice is lost as heat, while energy transported through charge carriers may be used to drive an optoelectronic circuit (*1*). Nanoscale systems can offer various ways to control energy relaxation pathways, potentially resulting in more efficient device operation. Novel relaxation pathways that result from electron confinement have been demonstrated in nanocrystal quantum dots and carbon nanotubes (*2*, *3*). In graphene, energy relaxation pathways are strongly altered by the vanishing electronic density of states (*4*–*6*). After initial relaxation of photoexcited carriers (as a result of electron-electron scattering and optical phonon emission), electron-lattice energy relaxation can be quenched (*4*), which creates a bottleneck that limits further energy redistribution into the lattice. With electron-to-lattice energy relaxation quenched, a novel transport regime is reached in which thermal energy is redistributed solely

[1]Department of Physics, Massachusetts Institute of Technology, Cambridge, MA 02139, USA. [2]Harvard School of Engineering and Applied Sciences, Harvard University, Cambridge, MA 02138, USA. [3]Department of Physics, Harvard University, Cambridge, MA 02138, USA. [4]National Institute for Materials Science, Namiki 1-1, Tsukuba, Ibaraki 305-0044, Japan.

*To whom correspondence should be addressed. E-mail: pjarillo@mit.edu